Limits of emission quantum yield determination

van Dam, B.; Bruhn, B.; Dohnal, G.; Dohnalová, K.

Limits of emission quantum yield determination

Bart van Dam,[1] Benjamin Bruhn,[1] Gejza Dohnal,[2] and Kateřina Dohnalová[1,a]

[1]*University of Amsterdam, Institute of Physics, Science Park 904, 1098 XH Amsterdam, The Netherlands*

[2]*Czech Technical University in Prague, Faculty of Mechanical Engineering, Karlovo náměstí 13, 121 35 Prague 2, Czech Republic*

The development of new fluorescent molecules and dyes requires precise determination of their emission efficiency, which ultimately defines the potential of the developed materials. For this, the photoluminescence quantum yield (QY) is commonly used, given by the ratio of the number of emitted and absorbed photons, where the latter can be determined by subtraction of the transmitted signal by the sample and by a blank reference. In this work, we show that when the measurement uncertainty is larger than 10% of the absorptance of the sample, the QY distribution function becomes skewed, which can result in underestimated QY values by more than 200%. We demonstrate this effect in great detail by simulation of the QY methodology that implements an integrating sphere, which is widely used commercially and for research. Based on our simulations, we show that this effect arises from the non-linear propagation of the measurement uncertainties. The observed effect applies to the measurement of any variable defined as $Z = X/Y$, with $Y = U - V$, where X, U and V are random, normally distributed parameters. For this general case, we derive the analytical expression and quantify the range in which the effect can be avoided. © *2018 Author(s). All article content, except where otherwise noted, is licensed under a Creative Commons Attribution (CC BY) license (http://creativecommons.org/licenses/by/4.0/).* https://doi.org/10.1063/1.5023295

I. INTRODUCTION

The photoluminescence quantum yield (QY) is commonly applied to quantify the emission efficiency of fluorescent molecules and dyes in their development for lighting applications. The QY is given by the ratio of the number of emitted N_{em} and absorbed N_{abs} photons, where the absorption is commonly obtained by comparison of the total number of photons transmitted by the sample (N_S) and a blank reference (N_{Ref}):

$$QY = \frac{N_{em}}{N_{abs}} = \frac{N_{em}}{N_{Ref} - N_S} \tag{1}$$

The QY is widely used also in research: In the past decade, research on quantum dot 'phosphors' has been relying on the QY methodology to show various size-,[1–3] excitation-[4–7] or concentration-dependent properties.[4,8] Several guidelines exist for the QY measurements,[9,10] discussing e.g. the effects of re-absorption[11] and excitation geometry.[12,13] However, none of them reflect on the critical effect of low sample absorption in the presence of measurement uncertainty - which can lead to dramatically biased results, as will be discussed here.

In this work we show that when the magnitude of the difference between the signals of the reference and sample measurement, used to evaluate the QY, reach levels comparable to that of experimental uncertainty (e.g. noise), the QY value can be heavily underestimated. This happens already under common experimental conditions, especially when absorption of the sample is relatively weak. For example, for noise levels of ∼ 1% the QY estimates for samples with an absorptance[14]

---

[a]corresponding author: k.newell@uva.nl, Presently: Katerina Newell

below ∼ 10% are affected. The effect is analyzed here in a great detail by simulating the QY methodology using an analytical model with careful consideration of the involved measurement uncertainties. We show that the uncertainty in the variables used to estimate the QY propagates in a non-linear way and leads, not only to a larger uncertainty in the QY value as is commonly assumed, but also to a considerable underestimation of the most-likely observed QY. This underestimation arises purely from the form in which the QY is defined, given by the general relation X/Y, and shows in case the denominator $Y = (U - V)$ is small. Therefore, our findings can be extended to any quantity determined by such type of a relation.

II. QY METHODOLOGY

We choose to demonstrate this effect on the QY method. To this end, we developed an analytical model to simulate the QY experiment. For this we select the optical QY methodology introduced by *Greenham*[15] and *de Mello et al.*,[16] and simplified by *Mangolini et al.*[17] This technique implements an integrating sphere (IS), a reflectively scattering cavity, that allows the determination of the absolute number of emitted and absorbed photons, without the need for a QY calibration standard. The use of the IS has been standardized for LED and display industry, and QY devices based on the IS methodology are commercially available.[18,19] Our model assumes a simplified and generalized IS geometry as shown in Figure 1, implementing the experimental scheme described by *Mangolini et al.*[17] In this method, a sample (e.g. a cuvette containing a solvent in which emitting nanoparticles are dispersed) is suspended inside the IS and excited from the entrance port. The excitation photons
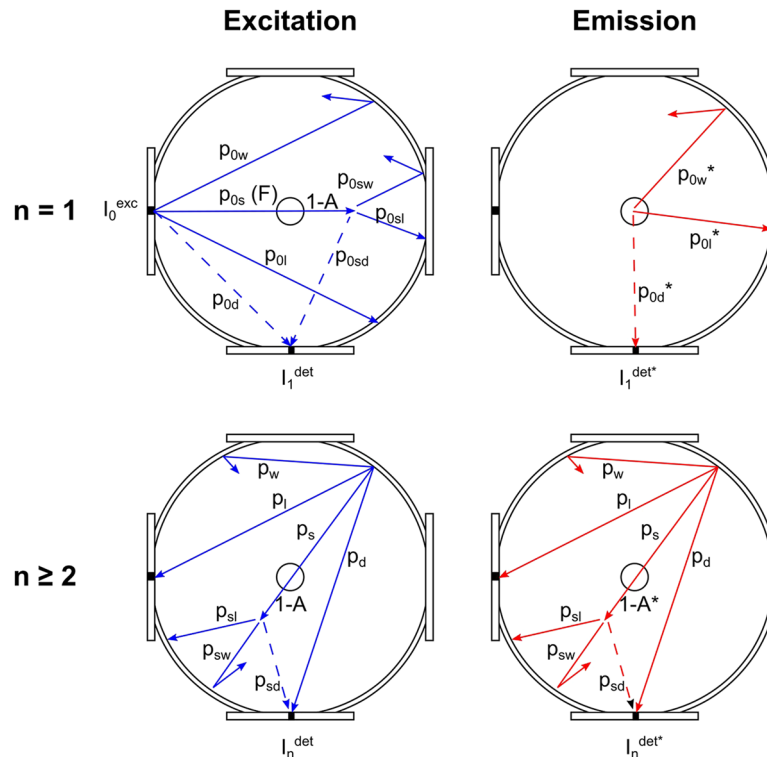

FIG. 1. Schematics of a generalized integrating sphere (IS) setup used for our model. The IS cavity has a small entrance on the left side and an exit on the bottom side, where a detector is placed. The sample/reference is modelled as a spherical object suspended in the center. Lines represent the light paths between different objects inside the IS - wall (w), loss channel (l), detector (d) and sample (s). The parameters represent the probabilities of taking each specific light path. Light paths shown in dashed lines are prevented by the screen (so called 'baffles'). The light paths before the first reflection from the IS wall ($n = 1$) are considered separately to account for the inhomogeneity of the light field in that instance. This differs for excitation light (entering from outside) and emission (originating from the center). Emission (red lines) is assumed separately from the excitation (blue lines) due to different spectral ranges, where the reflectivity of the sphere and the sample's absorption differ.

that are absorbed by the sample, are subsequently emitted at a different wavelength, with a probability given by the quantum efficiency η. After multiple reflections and scattering events within the IS, the excitation and emission photons are ultimately detected, lost or (re-) absorbed in the sample. The same measurement is repeated with a blank reference sample (e.g. the cuvette with solvent). From the difference in detected photon intensities at the excitation wavelengths (I) and emission wavelengths (I^*), the numbers of absorbed and emitted photons are evaluated:

$$QY = \frac{N_{em}}{N_{abs}} = \frac{N_S^* - N_{Ref}^*}{N_{Ref} - N_S} = \frac{\int (I_S^* - I_{Ref}^*) C^* \mathrm{d}t}{\int (I_{Ref} - I_S) C \mathrm{d}t}, \tag{2}$$

where subscripts S and *Ref* refer to the sample and reference measurements. The factors C and C^* correct for the spectral sensitivity of the detector and IS at the excitation and emission wavelength, respectively. For this an additional calibration measurement is performed using an empty IS and a calibration source with a known spectrum.

III. ANALYTICAL MODEL

We model the IS as a spherical cavity with two small openings: an entrance port from which excitation light enters and an exit port equipped with a detector. The sample or reference is suspended in the middle of the IS and is modeled as a spherical object with absorptance A, reflectance R and transmittance T, where $A + R + T = 1$. The interior of the IS is covered by a coating that is highly reflective over a broad spectral range R_w (usually > 97%) and acts as an ideal scatterer, i.e. the directionality of the light is lost after a single reflection from the walls. We define the probability p that a photon impinges on an object inside the IS by the relative area of the object to the area of the IS interior. For example the probability of hitting the wall (p_w), loss channel (p_l), detector (p_d) or sample (p_s), with $1 = p_l + p_d + p_s + p_w$. Since the ideally scattering walls ensure spatially distribution of the photons, we assumed that these probabilities do not depend on the exact location in the IS at which the photon scatters. However, to take into account that all the light starts from a single point (i.e. excitation from the entrance port and emission from the sample), we separate the first round of light reflection ($n = 1$) from the consequent ones ($n \geq 2$) (see Figure 1). We do this by assigning modified probabilities p_{0x} of hitting objects inside the IS, given by their visibility from the entrance. Again, $1 = p_{0l} + p_{0d} + p_{0s} + p_{0w}$ and $1 = p_{0w}^* + p_{0l}^* + p_{0d}^*$. p_{0s} represents the fraction of the initial excitation light intensity, I_0^{exc}, that hits the sample directly, a parameter that is commonly varied in literature.[12,13,16] To separate this parameter from the other probabilities, we set $p_{0s} = F$, where $F = 1$ for direct or $F = 0$ for indirect excitation conditions. Furthermore, in accordance with the standard IS methodology, direct detection of the excitation and emission photons is prevented by an inserted baffle by setting $p_{0sd} = p_{sd} = p_{0d} = p_{0d}^* = 0$ (dashed lines in Figure 1). For the sake of completeness, we finally assume that the measurement is in a regime in which the QY is independent of the excitation photon flux.

From the light paths illustrated in Figure 1 and their probabilities p_x, we simulate the transmitted excitation intensities during the first ($n = 1$) up to the n-th reflections:

$$I_1^{exc} = I_0^{exc}[p_{0w} + F(1 - A)p_{0sw}]R_w$$

$$I_2^{exc} = I_1^{exc}[p_w + p_s(1 - A)p_{sw}]R_w$$

$$I_3^{exc} = I_2^{exc}[p_w + p_s(1 - A)p_{sw}]R_w$$

$$\vdots$$

$$I_n^{exc} = I_{n-1}^{exc}[p_w + p_s(1 - A)p_{sw}]R_w$$

$$= I_0^{exc}[p_{0w} + F(1 - A)p_{0sw}]R_w$$

$$\times \{[p_w + p_s(1 - A)p_{sw}]R_w\}^{n-2}.$$

Here, p_{0sw} and p_{sw} indicate the probabilities of light passing through the sample and hitting the wall for the first and consecutive reflections, respectively. Similarly, we evaluate the absorbed intensity

(I^{abs}) by the sample/reference and the intensity recorded by the detector (I^{det}) at the exit of the IS by:

$$I_1^{abs} = I_0^{exc} FA$$
$$I_n^{abs} = I_{n-1}^{exc} p_s A$$
$$I_1^{det} = I_0^{exc} [p_{0d} + F(1-A)p_{0sd}]$$
$$I_n^{det} = I_{n-1}^{exc} [p_d + p_s(1-A)p_{sd}].$$

For the emitted light intensity (I^{em}) and its fraction recorded by the detector (I^{det^*}), we consider a different reflectivity of the IS coating R_w^* and an effective sample absorptance A^*:

$$I_1^{em} = I_0^{em} p_{0w}^* R_w^*$$
$$I_n^{em} = I_{n-1}^{em} R_w^* [p_w + p_s(1-A^*)p_{sw}]$$
$$I_1^{det^*} = I_0^{em} p_{0d}^*$$
$$I_n^{det^*} = I_{n-1}^{em} [p_d + p_s(1-A^*)p_{sw}].$$

To account for re-absorption and subsequent re-emission, A^* is defined as $A^* = A(\lambda_{em})(1-\eta)$, i.e. the fraction that is absorbed by the sample, but not re-emitted. The initial emission intensity originating from the sample is given by $I_0^{em} = I_{tot}^{abs} c\eta$, where I_{tot}^{abs} is the total excitation intensity absorbed in the sample and c is the fraction of light absorbed by the emitters in the sample (i.e. $c < 1$ when the emitters are dispersed in an absorbing matrix or solvent). The total absorbed intensity by the sample during the measurement is calculated by summation of I_n^{abs} over all reflection-steps. Using the geometric series, $\sum_{n=0}^{\infty} x^n = \frac{1}{1-x}$, we obtain:

$$I_{tot}^{det} = \sum_{n=1}^{\infty} I_n^{det} = I_0^{exc} \left\{ p_{0d} + F(1-A)p_{0sd} + R_w[p_{0w} + F(1-A)p_{0sw}] \frac{p_d + p_s(1-A)p_{sd}}{1 - R_w[p_w + p_s(1-A)p_{sw}]} \right\} \quad (3)$$

$$I_{tot}^{abs} = \sum_{n=1}^{\infty} I_n^{abs} = I_0^{exc} A \left\{ F + R_w[p_{0w} + F(1-A)p_{0sw}] \frac{p_s}{1 - R_w[p_w + p_s(1-A)p_{sw}]} \right\} \quad (4)$$

$$I_{tot}^{det^*} = \sum_{n=1}^{\infty} I_n^{det^*} = I_0^{em} \left\{ p_{0d}^* + p_{0w}^* R_w^* \frac{p_d + p_s(1-A^*)p_{sd}}{1 - R_w^*[p_w + p_s(1-A^*)p_{sw}]} \right\}. \quad (5)$$

For the spectral sensitivity correction factors C and C^* we assume an empty sphere ($A = 0$) and compare the theoretical intensity, equal to the input intensity at the sphere entrance I_0^{exc}, with the detected intensity at the sphere exit. This is done separately for the excitation and emission wavelengths, where in the latter case we replace R_w by R_w^*.

$$C = \frac{I_0^{exc}}{I_{det}^{tot}(A=0)} = \left[p_{od} + F p_{0sd} + R_w(p_{0w} + F p_{0sw}) \frac{p_d + p_s p_{sd}}{1 - R_w(p_w + p_s p_{sw})} \right]^{-1}. \quad (6)$$

Assuming that the reference sample does not emit ($N_{Ref}^* = 0$), the QY is given by:

$$QY = \frac{N_{em}}{N_{abs}} = \frac{\int I_{tot}^{det^*}(A_S)C^* dt}{\int [I_{tot}^{det}(A_{Ref}) - I_{tot}^{det}(A_S)]C dt} \quad (7)$$

For common IS conditions, such as a non-absorbing reference ($A_{Ref} = 0$), no re-absorption ($A_S^* = 0$) and inserted baffles ($p_{0d} = p_{0sd} = p_{0d}^* = p_{sd} = 0$), the number of emitted N_{em} and absorbed N_{abs} photons in Equation (7) can be expressed as:

$$N_{em} = N_S^* = \int I_0^{exc} [F + (p_{0w} + F(1-A_S)p_{0sw})Mp_s]A_S\eta \frac{p_{0w}^* M^* p_d}{(p_{0w} + F p_{0sw})M_{cal}^* p_d} dt \quad (8)$$

$$N_{abs} = N_{Ref} - N_S = \int I_0^{exc} \left[1 - \frac{(p_{0w} + F(1-A_S)p_{0sw})Mp_d}{(p_{0w} + F p_{0sw})M_{cal}^* p_d} \right] dt. \quad (9)$$

The parameters M and M^* are 'sphere-multipliers', defined as $M = R_w(1 - R_w[p_w + p_s(1-A)p_{sw}])^{-1}$ and $M^* = R_w^*(1 - R_w[p_w + p_s(1-A)p_{sw}])^{-1}$ and describe how light is distributed over the IS interior

and the objects inside it.[10] For the calibration measurements, $M_{cal} = M(A = 0)$ and $M^*_{cal} = M^*(A = 0)$. Assuming that loss channels are small, $p_{0w} = 1 - F - p_{0l} \sim 1 - F$, Equations (8) and (9) reduce to the QY descriptions found elsewhere.[10,12,16] In addition, the validity of our analytical approach has been separately verified using ray-tracing simulations.

IV. RESULTS

Using the procedure outlined above, we simulate the QY that would be measured in a typical QY geometry, for which we select an IS with a diameter of 10 cm, a reflectance at the excitation and emission wavelengths of 0.97 and 0.99 and set the diameter of the sample, input port and output to 1 cm, 4 mm and 1 mm respectively. The reference sample is assumed to be non-absorbing and non-emitting ($A_{Ref} = 0$ and $N^*_{Ref} = 0$) and the sample emission efficiency is set to an arbitrary value of $\eta = 80\%$. To account for measurement uncertainties in the number of detected excitation and emission photons, we describe those variables by a distribution function with an expectation value determined by Equations (3) and (5) (Figure 2a). The peak of the distribution indicates the most-likely value of the variable, whereas the standard deviation of the distribution σ indicates its fluctuations.

To cover commonly encountered measurement uncertainties, we discuss two types of distributions: A Poisson and a normal distribution. The Poisson distribution is given by $P(k, \mu) = \frac{\mu^k e^{-\mu}}{k!}$, where μ is the expected value and $P(k, \mu)$ the probability of measuring a photon count value $k = 0, 1, 2, 3,$ …. It is used to describe shot noise, which arises from the discrete nature of photons and will show especially for low flux signals, since the signal-to-noise ratio of the Poisson distribution increases with the square root of the number of detected photons ($\sqrt{N}$). The normal distribution is given by $G(k, \mu, \sigma^2) = \frac{e^{-\frac{(k-\mu)^2}{2\sigma^2}}}{\sqrt{2\pi\sigma^2}}$, where μ is again the expected (mean) value, σ^2 is the variance and k is the variable, i.e. photon counts. The normal distribution can be used to model measurement uncertainties that arise from e.g. mechanical/electronic stability of the detection and excitation chains and describes a more general situation in which the variance σ^2 can be set independently from the expectation value μ.

In typical QY experiments, the recorded counts N_{Ref} and N_S are usually very high (10^5 photon counts or more) and can otherwise easily be increased, by extending the measurement time or by doing multiple runs of the same measurement. As a consequence, the scenario in which (Poissonian) shot noise dominates the signal is unlikely in practice. Moreover, for higher photon fluxes the Poisson distribution can be well approximated by a normal distribution $P(k, \mu) \sim G(k, \mu, \mu)$. We therefore choose to discuss the fluctuations resulting from a normal distribution of the measured variables, to describe a more general source of experimental uncertainty in QY measurements. We will confine the specific case of Poisson distributed variables to the supplementary material.

To study the effect of measurement uncertainty on the QY, we simulate the distribution of the number of detected photons N_S, $N^*_S \equiv N_{em}$ and N_{Ref} by drawing semi-randomly from a normal distribution, $N_S \sim G(k, \mu_S, \sigma^2_S)$, $N^*_S \sim G(k, \mu_{S^*}, \sigma^2_{S^*})$ and $N_{Ref} \sim G(k, \mu_{Ref}, \sigma^2_{Ref})$. We set the standard deviation of each variable by choosing a fixed value of the relative uncertainty, α, defined as $\alpha = \frac{\sigma}{\mu}$, i.e. the fluctuation in the measured variables relative to the mean value. The distributions are illustrated for $\alpha = 1\%$ (green) and $\alpha = 0.1\%$ (black) in Figure 2a. Using Equation (2) we then compute the QY distribution, shown for different values of α in Figure 2b. For a low uncertainty α (black curve), the simulated distribution of the number of absorbed photons $N_{abs} = N_{Ref} - N_S$ is narrow, which leads to a QY distribution that lies symmetrically around the expected QY value (dashed vertical line). Upon increasing α (green curve), however, the distribution of N_{abs} broadens with one tail approaching zero, and the QY distribution ($QY \propto 1/N_{abs}$) becomes asymmetric. In this case, the most-likely QY value (the peak of the distribution) is shifted towards lower, underestimated values. Moreover, there is a finite probability of finding negative QY values when $N_S > N_{Ref}$. A similar effect occurs when α is fixed and the absorptance is varied, as shown for in Figure 2c. For an absorptance of 1%, the most-likely QY estimate is underestimated by more than a factor of ~ 2, i.e. 200%. The absorption value for which the QY is underestimated strongly depends on the relative uncertainty of the measurement as shown in Figure 2d. For $\alpha = 0.1\%$, the most-likely QY agrees very well with
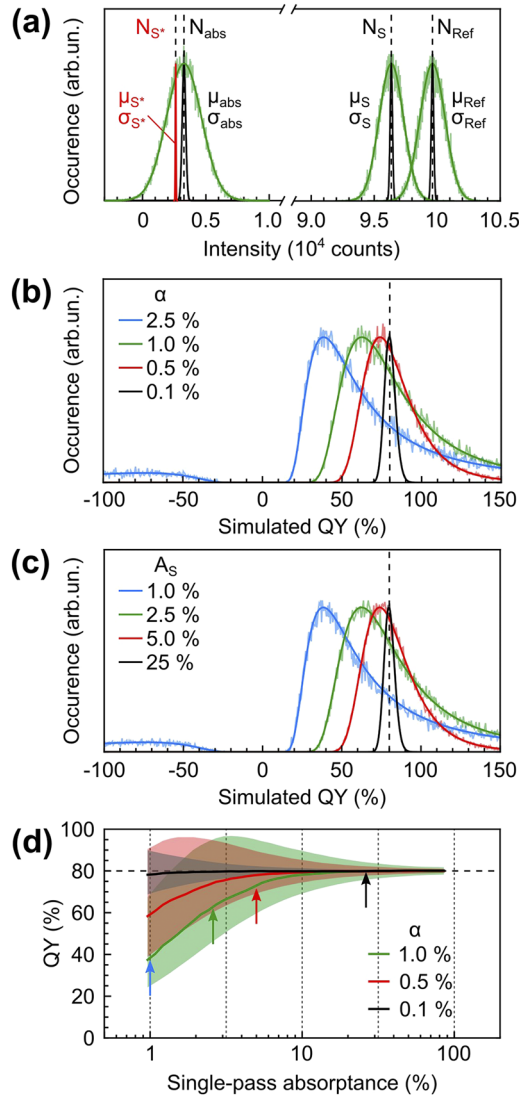
FIG. 2. Simulated effect of normally distributed noise on the QY: (a) Normalized histograms of the number of detected emission photons N_{em} (red) and excitation photons N_S and N_{Ref} for a sample absorptance of 2.5% (black and green). The latter are shown for a relative measurement uncertainty of 1% (green) and 0.1% (black). The thick solid lines show normal distributions; the vertical dashed lines indicate the (noiseless) most-likely values. (b) Normalized histograms of the simulated QY values for a fixed sample absorptance ($A_S \sim 2.5\%$) and different relative measurement uncertainties and (c) for a fixed measurement uncertainty ($\alpha = 1\%$) and a varying sample absorptance. The thick solid lines in (b, c) indicate fits by the analytical expression for the ratio-distribution (Equation (10)). (d) The simulated most-likely QY value (lines) and the full-width at half-maximum (FWHM) of the positive part of the simulated QY distribution (shaded regions) against the single-pass absorptance of the sample. The horizontal dashed line shows the simulated QY without added noise. Relative uncertainties are set to $\alpha = 1, 0.5$ and 0.1%. The arrows indicate the absorptance values used in panel (c).

the expected QY, independent of the absorption of the sample. However, already for the relative uncertainties of 0.5%, the QY estimate is reliable only when the sample's absorptance exceeds ~5%. For even higher uncertainties of 1%, the absorption limit is as high as ~15%.

V. DISCUSSION

Figure 2b–d shows that the QY distribution becomes skewed when the fluctuations in the number of detected photons become comparable to the one tenth of the absorptance of the sample: $\alpha/A_S \sim 10\%$. This results in a large variance in the number of absorbed photons (N_{abs}, Figure 2a),
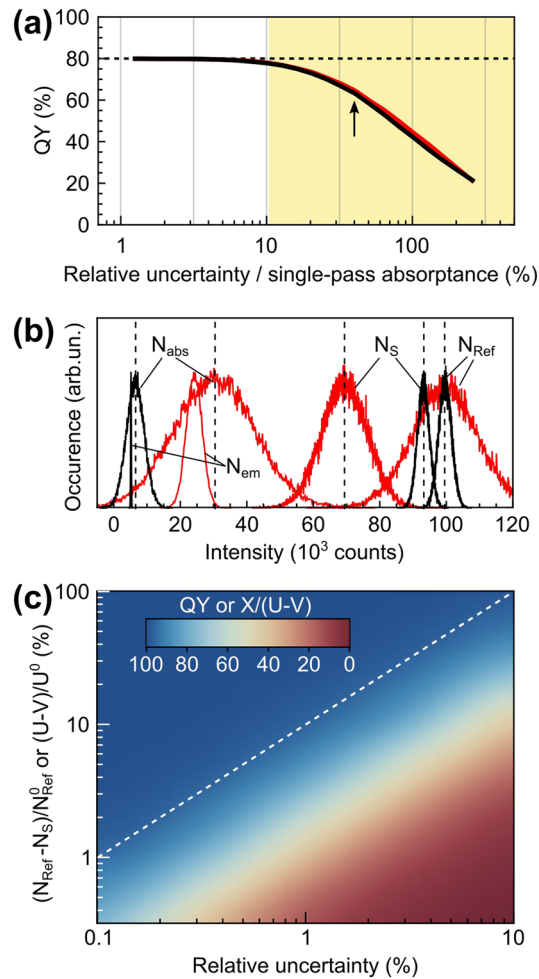
FIG. 3. (a) Simulated most-likely QY value against the relative measurement uncertainty, normalized to the sample's single-pass absorptance A_S for $A_S = 5\%$ (black) and $A_S = 25\%$ (red). The horizontal dashed black line indicates the noiseless QY value. For a relative noise level of $> 10\%$ of the single-pass absorptance value, the QY is underestimated (yellow area). The arrow indicates the situation in panel (b). (b) Simulated distribution of N_{Ref}, N_S and $N_{abs} = N_{Ref} - N_S$ for $A_S = 5\%$ and $\alpha = 2\%$ (black) and $A_S = 25\%$ and $\alpha = 10\%$ (red). (c) QY (color bar) as a function of the normalized number of absorbed photons $(N_{Ref} - N_S)/N_{Ref}^0$ and relative uncertainty in the N_{Ref} and N_S estimates. The dashed white line indicates the threshold below which the QY is unreliable. This holds for any quantity given by the general relation $X/(U - V)$.

which due to the inverse proportionality $QY \propto 1/N_{abs}$ results in an skewed distribution function of the QY. The relative fluctuations in the number of emitted photons, given by the same α, are small (Figure 3b). Moreover, since N_{em} is in the nominator of the QY definition (Equation (1)), it therefore has a negligible effect on the shape of the QY distribution. The full dependence of the QY on the relative uncertainty and absorptance is shown in Figure 3a for samples with a single-pass absorptance of 5% (black) and 25% (red). When α is small compared to the absorptance, $\alpha/A_S < 10\%$, the most-likely QY is in good agreement with the unbiased result, whereas for $\alpha/A_S > 10\%$ (yellow area) the QY is increasingly underestimated. For α equal to the sample's single-pass absorptance, the most-likely QY is already reduced to 50% of the unbiased value. A nearly identical curve is obtained for an arbitrary absorption value, even when the absorptance is high (red curve). In both cases, there is a large variance in the distribution of N_{abs} (Figure 3b). This shows that it is the ratio of the relative uncertainty and the sample absorption that determines the underestimation of the QY.

An another important finding it that in the ideal case, in which noise is absent, the IS methodology itself does not yield biased results. The bias (Figure 2) arises only when accounting for the measurement uncertainty in the simulated number of detected photons predicted by Equations (3)

and (5). Hence we conclude that the bias results purely from the relation from which the QY and, in particular, the absorption part of the QY is determined: $QY \propto 1/(N_{Ref} - N_S)$. The same effect is therefore expected to show for any quantity with the general form $Z = X/Y$ and $Y = U - V$, when the uncertainty in U and V is comparable to the value of $(U - V)$.

We can derive the analytical expression for the probability distribution of this general case. By taking normally distributed random variables $X \sim G(k, \mu_X, \sigma_X^2)$, $U \sim G(k, \mu_U, \sigma_U^2)$ and $V \sim G(k, \mu_V, \sigma_V^2)$, we get $Y \sim G(k, \mu_Y, \sigma_Y^2)$ with $\mu_Y = \mu_U - \mu_V$ and variance $\sigma_Y^2 = \sigma_U^2 + \sigma_V^2$. It then follows that the derived ratio $Z = X/Y$ is a continuously distributed random variable with the probability density function (for more details, see the supplementary material):[20]

$$p_Z(z) = \frac{\theta}{\pi(z^2 + \theta^2)}[\sqrt{2\pi}B(z)\Phi(B(z))e^{-\frac{C(z)}{2}} + K], \tag{10}$$

where

$$B(z) = \frac{\alpha_Y z + \alpha_X \theta}{\alpha_X \alpha_Y \sqrt{z^2 + \theta^2}}$$

$$\Phi(z) = \int_{-\infty}^{z} \frac{1}{\sqrt{2\pi}} e^{-\frac{1}{2}u^2} du$$

$$C(z) = \frac{(\alpha_Y \theta - \alpha_X z)^2}{\alpha_X^2 \alpha_Y^2 (z^2 + \theta^2)}$$

$$K = \exp(-\frac{\alpha_X^2 + \alpha_Y^2}{2\alpha_X^2 \alpha_Y^2}).$$

Here, we again define the relative uncertainty $\alpha_i = \sigma_i/\mu_i$ with $i = X, Y, U, V$ and the parameter $\theta = \sigma_X/\sigma_Y$. For simplicity, we assume that the measurements of variables X, Y, U and V are all independent, which typically holds for QY measurements. The general case with dependent variables is discussed in the supplementary material.

The first factor in Equation (10) is the 'standard' part of the density of a non-centered Cauchy distribution, which is independent of $\mu_{X,Y}$ and has no mean or variance. The factor in brackets is known as the 'deviant' part, and leads to the skewed shape of the distribution. Using the analytical expression in Equation (10), we can very precisely fit our simulated QY distributions in Figure 2b,c (colored full lines), thus validating our results.

Finally, in Figure 3c we summarize the limitations of the determination of the QY (or any analogous quantity $Z = X/(U - V)$) by plotting the general dependence of the most-likely QY (Z) on the relative measurement uncertainty α and the absorptance A_S (or general analogue to absorptance $(U - V)/U^0$), i.e. the fraction of the number of incident photons N_{Ref}^0 that is absorbed by the sample, $(N_{Ref} - N_S)/N_{Ref}^0$. The threshold below which the QY estimate becomes unreliable is designated by the white dotted line in Figure 3c and corresponds to the yellow area in Figure 3a. As a rule of thumb, the QY can be reliably estimated for a sample with an absorptance that exceeds ∼10% of the relative measurement uncertainty, e.g. for an absorptance > 1% when $\alpha = 0.1\%$. The QY becomes unreliable upon decreasing absorption or increasing measurement uncertainty.

VI. CONCLUSION

In conclusion, we report on a general issue arising in experimental methodologies where a quantity in the form $Z = X/Y$ with small $Y = U - V$ is evaluated, such as the photoluminescence QY. These quantities are biased towards lower values when $(U - V)/U^0$ is ∼ 10% of the uncertainty in the variables U and V. This happens commonly in QY measurements of low-absorbing samples, since for typical noise levels of ∼ 1%, absorptance below 10% is already affected. Those numbers are not uncommon in many experiments, which suggests that this bias could have been present in published results that rely on the QY methodology.[2–4,12] This artifact has passed undetected for a long time, due to the assumption that the error in the measured signal intensities propagates in a linear manner and therefore that low photon fluxes, e.g. when measuring low-absorption or emission materials, merely result in a larger uncertainty in the obtained QY value.[10,21] The underestimation

arises purely from the uncertainty in the measured variables U and V compared to the normalized difference $(U - V)/U^0$. Hence we anticipate that, not only the absolute QY, but also the comparative and relative QY techniques will suffer from this effect. By detailed numerical simulations and by derivation of the skewed probability density function of the QY we quantify this effect and provide guidelines for the range of absorption values for which the QY can be reliably determined in each specific experimental setup.

SUPPLEMENTARY MATERIAL

See the supplementary material for a discussion of Poisson distributed variables, the full description of the ratio distribution and for experimentally determined QY distributions.

ACKNOWLEDGMENTS

[1] M. L. Mastronardi, F. Maier-Flaig, D. Faulkner, E. J. Henderson, C. Kubel, U. Lemmer, and G. A. Ozin, Nano Letters **12**, 337 (2012).

[2] J. B. Miller, A. R. van Sickle, R. J. Anthony, D. M. Kroll, U. R. Kortshagen, and E. K. Hobbie, ACS Nano **6**, 7389 (2012).

[3] W. Sun, C. Qian, L. Wang, M. Wei, M. L. Mastronardi, G. Casillas, J. Breu, and G. A. Ozin, Advanced Materials **27**, 746 (2015).

[4] D. Timmerman, J. Valenta, K. Dohnalová, W. D. A. M. de Boer, and T. Gregorkiewicz, Nature Nanotechnology **6**, 710 (2011).

[5] S. Saeed, E. M. L. D. de Jong, K. Dohnalova, and T. Gregorkiewicz, Nature Communications **5**, 4665 (2014).

[6] N. X. Chung, R. Limpens, and T. Gregorkiewicz, Advanced Optical Materials **5**, 1600709 (2017).

[7] J. Valenta, M. Greben, S. Gutsch, D. Hiller, and M. Zacharias, Applied Physics Letters **105**, 243107 (2014).

[8] M. Greben, A. Fucikova, and J. Valenta, Journal of Applied Physics **117**, 144306 (2015).

[9] C. Würth, M. Grabolle, J. Pauli, M. Spieles, and U. Resch-Genger, Nature Protocols **8**, 1535 (2013).

[10] J. Valenta, Nanoscience Methods **3**, 11 (2014).

[11] T. S. Ahn, R. O. Al-Kaysi, A. M. Müller, K. M. Wentz, and C. J. Bardeen, Review of Scientific Instruments **78**, 2005 (2007).

[12] D. O. Faulkner, J. J. Mcdowell, A. J. Price, D. D. Perovic, N. P. Kherani, and G. A. Ozin, Laser and Photonics Reviews **6**, 802 (2012).

[13] C. Wurth and U. Resch-Genger, Applied Spectroscopy **69**, 749 (2015).

[14] Defined as the fraction of the incident light that is absorbed.

[15] N. Greenham, I. Samuel, G. Hayes, R. Phillips, Y. Kessener, S. Moratti, A. Holmes, and R. Friend, Chemical Physics Letters **241**, 89 (1995).

[16] J. C. de Mello, H. F. Wittmannn, and R. Friend, Advanced Materials **9**, 230 (1997), arXiv:97/0302-O23 [0935-9648].

[17] L. Mangolini, D. Jurbergs, E. Rogojina, and U. Kortshagen, Journal of Luminescence **121**, 327 (2006).

[18] "Hamamatsu C9920-02G."

[19] "Horiba Quanta-phi."

[20] A. Cedilnik, K. Kosmelj, and A. Blejec, Metodoloski Zvezki **1**, 99 (2004).

[21] N. X. Chung, R. Limpens, and T. Gregorkiewicz, Proc. SPIE **9562**, 95620O (2015).